Int. J. Solids Structures Vol. 17, pp. 891–901, 1981
Printed in Great Britain.

0020-7683/81/090891-11$02.00/0
Pergamon Press Ltd.

RESPONSE OF AN ELASTICALLY EMBEDDED ROD SUBJECTED TO PERIODICALLY SPACED LONGITUDINAL FORCES†

R. PARNES‡

Department of Solid Mechanics, Materials and Structures, School of Engineering, Tel-Aviv University, 69978 Ramat-Aviv, Israel

(*Received* 8 *January* 1980; *in revised form* 11 *August* 1980)

Abstract—The dynamic response of buried pipelines to earthquakes is best expressed in terms of dynamic amplification factors, i.e. as the ratio of dynamic to static response. In the present paper, the system is represented by a model consisting of a cylindrical rod of radius a embedded in an elastic medium. The required interacting static response of rods subjected to periodic longitudinal forces at intervals L and acting in alternate directions, is obtained. Such a load pattern corresponds to the incoherent motion occuring in earthquakes.

The static displacements and interacting stresses of the system are established and are found to be dependent, for a given medium, on the ratio of stiffness of the medium and rod as well as on the aspect ratio a/L. Numerical results are presented for a series of rods governed by the above non-dimensional parameters.

1. INTRODUCTION

A problem which has received considerable attention in recent years has been the effect of earthquakes on buried pipes in the earth[1, 2]. In particular, attempts have been made to establish the degree of interaction within the pipe-soil system.

In order to demonstrate effectively the dynamic effects of earthquakes, the response is best expressed in terms of dynamic amplification factors. Thus it is necessary to obtain the static response to equivalent forces acting upon the pipe. In the present paper the static solution to an interacting pipe-soil system is established.

In the model considered below, it is assumed that longitudinal forces act at the joints of the pipe at periodic intervals L. The maximum destructive effect on the pipe is known to occur due to such forces acting in alternate directions and it is this case which is therefore considered.

The pipe is represented by a linear elastic bar and the soil by an elastic isotropic material. The static response is obtained in terms of the ratio of the moduli of the two elastic materials as well as in terms of an aspect ratio defined as the ratio of radius to length L. Numerical results for the bar displacements as well as stresses acting at the pipe-medium interface are presented for a range of governing parameters.

2. GENERAL FORMULATION AND SOLUTION

The model considered is that of an infinite cylindrical elastic rod of radius a embedded in an infinite elastic medium and which is subjected to static concentrated forces F_0 acting in the axial z-direction at periodic intervals L as shown in Fig. 1.

The rod is represented by means of a cylindrical bar of cross-sectional area A, with modulus of Elasticity, E, whose motion in the longitudinal z-direction is denoted

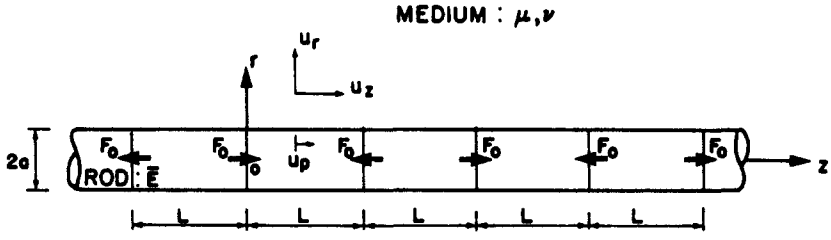

Fig. 1. Geometry of problem.

†This work was performed under a grant from the National Science Foundation, Washington, D.C. (Grant No. PFR 78–15049) with Weidlinger Associates, New York, U.S.A.

‡Presently on leave at l'Ecole Polytechnique, Laboratoire de Mécanique des Solides, 91128 Palaiseau, France.

by $u_p(z)$. Furthermore, following the assumption of radial rigidity[3], the radial displacements u_r are taken as zero throughout the bar.

The surrounding medium is assumed to behave as a linear isotropic elastic material defined by a shear modulus μ and Poisson ratio ν. For the axi-symmetric case considered here, the medium can undergo radial and axial displacements, denoted by $u_r(r, z)$ and $u_z(r, z)$ respectively.

The interaction between the bar and surrounding medium is then due to an interaction shear force mechanism which acts at the bar-medium interface and which tends to restrain the longitudinal motion.

Denoting the applied concentrated forces by means of periodically spaced Dirac-delta functions $\delta_p(z)$, the governing equation of the rod is then written as

$$\bar{E}\frac{\partial^2 u_p(z)}{\partial z^2}+\frac{2\tau_{rz}(a, z)}{a}=-\frac{F_0}{A}\delta_p(z) \tag{1}$$

where $\tau_{rz}(a, z)$ represented the interacting shear stress at the interface.

With the assumptions stated above, together with the requirements on continuity of displacements at the interface, the boundary conditions on the medium displacements become

$$u_r(a, z)=0,\ u_z(a, z)=u_p(z). \tag{2a,b}$$

The behavior of the surrounding medium can be readily formulated in terms of a Love strain function $\psi(r, z)$[4]. Expressing the radial and axial displacements of the medium for the axi-symmetric case respectively by

$$u_r=-\frac{1}{2\mu}\frac{\partial^2\psi}{\partial r\partial z} \tag{3a}$$

$$u_z=\frac{1-\nu}{\mu}\nabla^2\psi-\frac{1}{2\mu}\frac{\partial^2\psi}{\partial z^2}, \tag{3b}$$

the equations of equilibrium in the medium are then satisfied if

$$\nabla^4\psi(r, z)=0 \tag{4}$$

Appropriate solutions of the bi-harmonic equation which decay as $r\to\infty$ are[5]

$$\psi(r, z)=\sum_{m=1}^{\infty}X_m(r)\cos\alpha_m z \tag{5}$$

where

$$X_m(r)=A_mK_0(\alpha_m r)+B_m rK_1(\alpha_m r). \tag{6}$$

In the above, $K_n(\alpha_m r)$ are modified Bessel functions of the second kind.

Substitution in eqns (3) yields

$$u_r(r, z)=\sum_{m=1}^{\infty}u_{rm}(r, z)=-\frac{1}{2\mu}\sum_{m=1}^{\infty}\alpha_m{}^2[A_mK_1(\alpha_m r)+B_m rK_0(\alpha_m r)]\sin\alpha_m z \tag{7}$$

$$u_z(r, z)=\sum_{m=1}^{\infty}u_{zm}(r, z)=\frac{1}{2\mu}\sum_{m=1}^{\infty}\alpha_m\{A_m\alpha_mK_0(\alpha_m r)+B_m[\alpha_m rK_1(\alpha_m r)-4(1-\nu)K_0(\alpha_m r)]\}\cos\alpha_m z \tag{8}$$

where A_m and B_m are unknown constants which must satisfy the boundary conditions eqns (2).

From the first of these, it follows that

$$A_m = -B_m a \frac{K_0(\alpha_m a)}{K_1(\alpha_m a)}. \tag{9}$$

Furthermore, since $u_r(a, z) = 0$, the shear stress at the interface is given by

$$\tau_{rz}(a, z) = \mu \frac{\partial u_z(a, z)}{\partial r}. \tag{10}$$

Using the remaining boundary conditions and substituting eqn (10) in the bar equation, eqn (1) leads to an explicit equation for $u_z(a, z) = u_p(z)$:

$$\bar{E} \frac{\partial^2 u_z(a, z)}{\partial z^2} + \frac{2\mu}{a} \frac{\partial u_z(a, z)}{\partial r} = -\frac{F_0}{A} \delta_p(z). \tag{11}$$

From eqns (8) and (9), substitution in the above yields the equation for B_m; viz.

$$\sum_{m=1}^{\infty} B_m \alpha_m^2 \left\{ \frac{\bar{E}}{2\mu} \alpha_m \left[\left\{ 4(1-\nu) + \alpha_m a \frac{K_0(\alpha_m a)}{K_1(\alpha_m a)} \right\} K_0(\alpha_m a) - \alpha_m a K_1(\alpha_m a) \right] + \frac{4(1-\nu)}{a} K_1(\alpha_m a) \right\} \cos \alpha_m z = -\frac{F_0}{A} \delta_p(z). \tag{12}$$

The periodic Dirac-delta function may now be represented in the region $0 \le z \le L$ by means of the infinite series

$$\delta_p(z) = \frac{2}{L} \sum_{m=1}^{\infty} \cos \alpha_m z \tag{13}$$

where

$$\alpha_m = (2m-1)\pi/L. \tag{14}$$

It is noted here in passing that the interval $0 \le z \le L$ represents a half Fourier interval and hence the analysis of the infinite rod problem is given by the solution in a periodic interval $0 \le z \le L$, with $\lambda = 2L$ being the total Fourier interval (see Fig. 2).

Using the representation of eqn (13) in eqn (12), the constants B_m are readily determined; viz.

$$B_m = -\frac{4F_0 K_1(\alpha_m a)}{A \alpha_m^2 \Omega_m} \cdot \frac{a}{L} \cdot \frac{\mu}{\bar{E}}$$

where

$$\Omega_m = \alpha_m a \{4(1-\nu) K_0(\alpha_m a) K_1(\alpha_m a) + \alpha_m a [K_0^2(\alpha_m a) - K_1^2(\alpha_m a)]\} + 8(1-\nu) \frac{\mu}{\bar{E}} K_1^2(\alpha_m a). \tag{16}$$

Upon evaluating the constants A_m and B_m, the displacements are known according to eqn

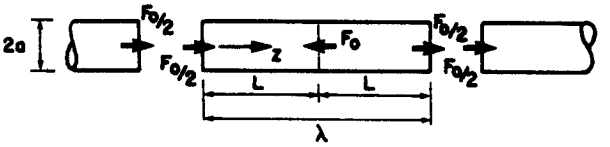

Fig. 2. Periodic interval.

(8). However at this point, it is advantageous to express the solution in terms of non-dimensional quantities. To this end, let

$$\eta = a/\lambda, \text{ where } \lambda = 2L \tag{17a}$$

$$R = \mu/\bar{E} \tag{17b}$$

$$v = \alpha_m a = 2\pi\zeta\eta, \text{ where } \zeta = 2m - 1 \tag{17c}$$

$$\rho = r/a, \quad \xi = z/L. \tag{17d,e}$$

Using these new non-dimensional parameters, and substituting the appropriate constants, we obtain:

$$\left(\frac{u_r(\rho, \xi)}{L}\right)\left(\frac{\bar{E}A}{F_0/2}\right) = 16\eta^2 \sum_{m=1}^{\infty} \frac{1}{\Omega_m(v)}\{\rho K_0(\rho v)K_1(v) - K_0(v)K_1(\rho v)\}\sin \pi\zeta\xi \tag{18a}$$

$$\left(\frac{u_z(\rho, \xi)}{L}\right)\left(\frac{\bar{E}A}{F_0/2}\right) = 4\eta^2 \sum_{m=1}^{\infty} \frac{1}{v\Omega_m(v)}\{4(1-\nu)K_0(\rho v)K_1(v) + v[K_0(\rho v)K_0(v) - \rho K_1(\rho v)K_1(v)]\}\cos \pi\zeta\xi \tag{18b}$$

where

$$\Omega_m(v) = v[4(1-\nu)K_0K_1 + v(K_0^2 - K_1^2)] + 8(1-\nu)RK_1^2. \tag{19}$$†

From the evaluated strain function $\psi(r, z)$ it is also possible to obtain the stresses throughout the surrounding medium from the following expressions [4]

$$\tau_{rr} = \frac{\partial}{\partial z}\left[\nu\nabla^2\psi - \frac{\partial^2\psi}{\partial r^2}\right] \tag{20a}$$

$$\tau_{\theta\theta} = \frac{\partial}{\partial z}\left[\nu\nabla^2\psi - \frac{1}{r}\frac{\partial\psi}{\partial r}\right] \tag{20b}$$

$$\tau_{zz} = \frac{\partial}{\partial z}\left[(2-\nu)\nabla^2\psi - \frac{\partial^2\psi}{\partial z^2}\right] \tag{20c}$$

$$\tau_{rz} = \frac{\partial}{\partial r}\left[(1-\nu)\nabla^2\psi - \frac{\partial^2\psi}{\partial z^2}\right]. \tag{20d}$$

Substitution of $\psi(r, z)$ in the above yields:

$$\frac{\tau_{rr}}{F_0/2A} = 16R\eta \sum_{m=1}^{\infty} \frac{1}{\rho\Omega_m}[\rho v K_0K_0(\rho v) + K_0K_1(\rho v) - \rho(2\nu - 1)K_0(\rho v)K_1 - \rho^2 v K_1K_1(\rho v)]\sin \pi\zeta\xi \tag{21a}$$

$$\frac{\tau_{\theta\theta}}{F_0/2A} = -16R\eta \sum_{m=1}^{\infty} \frac{1}{\rho\Omega_m}[K_0K_1(\rho v) + \rho(2\nu - 1)K_1K_0(\rho v)]\sin \pi\zeta\xi \tag{21b}$$

$$\frac{\tau_{zz}}{F_0/2A} = -16R\eta \sum_{m=1}^{\infty} \frac{1}{\Omega_m}[vK_0K_0(\rho v) + 2(2-\nu)K_1K_0(\rho v) - \rho v K_1K_1(\rho v)]\sin \pi\zeta\xi \tag{21c}$$

$$\frac{\tau_{rz}}{F_0/2A} = -16R\eta \sum_{m=1}^{\infty} \frac{1}{\Omega_m}[vK_0K_1(\rho v) - \rho v K_1K_0(\rho v) + 2(1-\nu)K_1K_1(\rho v)]\cos \pi\zeta\xi \tag{21d}$$

where $\Omega_m = \Omega_m(v)$ is defined in eqn (19).

It is noted that as $R = \mu/\bar{E}$ tends to zero, all stresses throughout the medium vanish as expected.

†In eqn (19), and in all subsequent equations, $K_n \equiv K_n(v)$.

3. DISPLACEMENTS AND STRESSES AT THE INTERFACE. NUMERICAL RESULTS

Setting $\rho = 1$, the displacements and stresses at the interface of the bar and surrounding medium simplify to:

$$u_r(1, \xi) = 0 \tag{22a}$$

$$\left[\frac{u_z(1, \xi)}{L}\right]\frac{\bar{E}A}{F_0/2} = 4\eta^2 \sum_{m=1}^{\infty} \frac{1}{v\Omega_m}[4(1-\nu)K_0K_1 + v(K_0^2 - K_1^2)]\cos \pi\zeta\xi \tag{22b}$$

$$\frac{\tau_{rr}(1, \xi)}{F_0/2A} = 16R\eta \sum_{m=1}^{\infty} \frac{1}{\Omega_m}[v(K_0^2 - K_1^2) + 2(1-\nu)K_0K_1]\sin \pi\zeta\xi \tag{22c}$$

$$\frac{\tau_{\theta\theta}(1, \xi)}{F_0/2A} = -32R\nu\eta \sum_{m=1}^{\infty} \frac{K_0K_1}{\Omega_m}\sin \pi\zeta\xi \tag{22d}$$

$$\frac{\tau_{zz}(1, \xi)}{F_0/2A} = -16R\eta \sum_{m=1}^{\infty} \frac{1}{\Omega_m}[v(K_0^2 - K_1^2) + 2(2-\nu)K_0K_1]\sin \pi\zeta\xi \tag{22e}$$

$$\frac{\tau_{rz}(1, \xi)}{F_0/2A} = -32R\eta(1-\nu) \sum_{m=1}^{\infty} \frac{K_1^2}{\Omega_m}\cos \pi\zeta\xi. \tag{22f}$$

A limiting case of particular interest for the bar displacement $u_p(\xi) = u_z(1, \xi)$ occurs when the surrounding medium becomes infinitely weak; i.e. $\mu \to 0$ or $R \to 0$. This case then represents a simple bar free to displace with no restraint from the surrounding medium. Letting $R \to 0$, and substituting for v and Ω_m, the displacement u_p becomes

$$\left(\frac{u_p(\xi)}{L}\right)\left(\frac{\bar{E}A}{F_0/2}\right) = \frac{4}{\pi^2} \sum_{m=1}^{\infty} \frac{\cos \pi\zeta\xi}{(2m-1)^2}. \tag{23}$$

At the point of load application, $\xi = 0$,

$$\left[\frac{u_p(\xi = 0)}{L}\right]\left[\frac{\bar{E}A}{F_0/2}\right] = \frac{4}{\pi^2} \sum_{m=1}^{\infty} \frac{1}{(2m-1)^2} = \frac{1}{2}, \tag{24a}$$

since the series [6]

$$\sum_{m=1}^{\infty} (2m-1)^{-2} = \pi^2/8. \tag{24b}$$

Note that here

$$u_p^f \equiv u_p(0)|_{R=0} = \frac{F_0L}{4A\bar{E}} \tag{25}$$

represents the displacement of a bar of length $2L$ in equilibrium under forces as shown in Fig. 2. The displacement at $z = L/2$ clearly vanishes and hence at $z = 0$ ($\xi = 0$) the displacement is as given by eqn (25). This displacement thus provides a physically meaningful quantity with respective to which it is possible to normalize the displacement u_p. Therefore, letting in general,

$$u^*(\xi) = \frac{u_p(\xi)}{u_p^f}, \tag{26}$$

from eqns (22b) and (25) one obtains, after some algebraic manipulation the explicit expression:

$$u^*(\xi) = \frac{8}{\pi^2} \sum_{m=1}^{\infty} \frac{\cos \pi\zeta\xi}{(2m-1)^2\left\{1 + \frac{2R}{v}\left[\frac{K_1^2(v)}{[K_0(v)K_1(v) + [v/4(1-\nu)]\{K_0^2(v) - K_1^2(v)\}]}\right]\right\}}. \tag{27}$$

Numerical results for the normalized longitudinal displacement and the stresses at the interface $r = a$ are presented for a medium with a Poisson ratio $\nu = 0.25$.

In Fig. 3, the variation of $u^*(\xi = 0)$, evaluated from eqn (27) as a function of $\eta = a/\lambda$, is shown for a family of stiffness ratios $R = \mu/\bar{E}$. From this figure, it is noted that for $\eta = 0$ (i.e. as the relative intervals separating the forces F_0 become infinite), the displacements vanish for all $R > 0$. As η increases, i.e. as the relative interval λ decreases, $u^*(\xi = 0)$ increases while remaining less than unity. For cases of a relatively weak medium, e.g. $R < 0.01$, a weak interaction exists and with increasing values of η, u^* approaches unity asymptotically; thus the behavior approaches that of a free rod. For larger values of R, stronger interaction occurs and is reflected in a greater attenuation of the displacement.

The relative effect of R and λ is demonstrated in Fig. 4 where the displacement u^* is plotted as a function of R for two typical values of η, $\eta = 0.05$ and 0.10. Here again, it is noted that the attenuation of the displacement is greater for small values of η. In a given system with $R = 0.5$, the attenuation with respect to a free rod is seen to be over 60% for values $\eta \leq 0.1$.

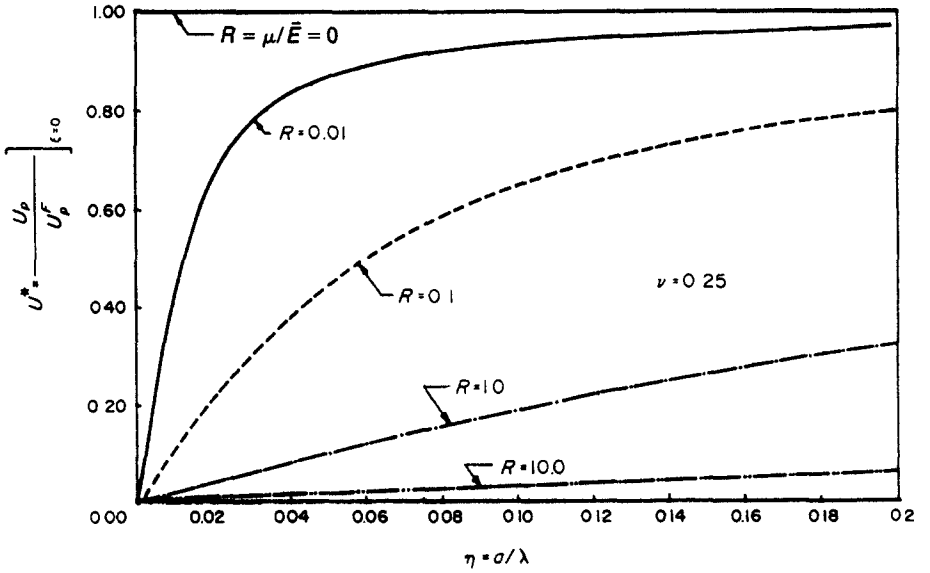

Fig. 3. Normalized displacement vs aspect ratio.

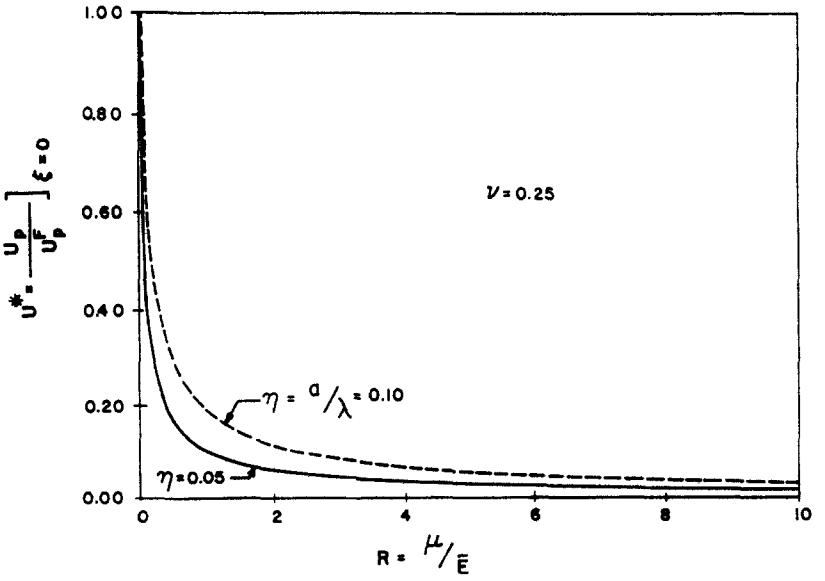

Fig. 4. Normalized displacement vs relative stiffness.

The variation of $u^*(\xi)$ along the longitudinal axis $\xi = z/L$†, obtained from eqn (22b), is shown in Fig. 5 for the case $\eta = 0.05$ and a family of values of R, while in Fig. 6, similar curves are presented with R held constant, $R = 1$. In both figures, it is observed that the displacement u^* at points away from the applied force varies linearly and increases more rapidly as ξ approaches zero.

The stresses acting at the interface, evaluated from eqns (22c–f), are shown in Figs. 7–11 and are plotted as a function of ξ, the position along the axis.

The variation of the interacting shear stress τ_{rz} is presented in Fig. 7 for a typical value $\eta = 0.05$ and for various stiffness ratios $R = 0.05, 0.1, 0.5$ and 1.0. The interacting shear stress is seen to be significant only for small values of $\xi = z/L$, namely only in the neighborhood of the

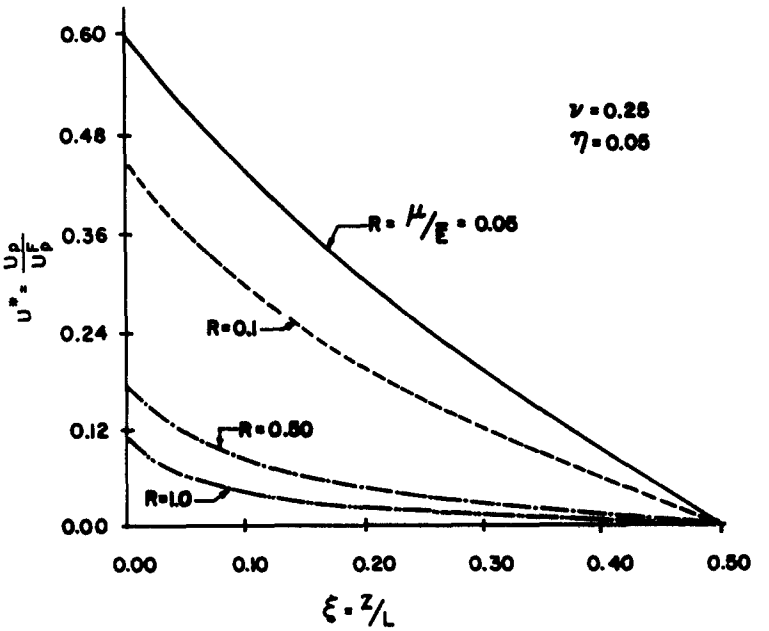

Fig. 5. Normalized displacement vs ξ, $\eta = 0.05$.

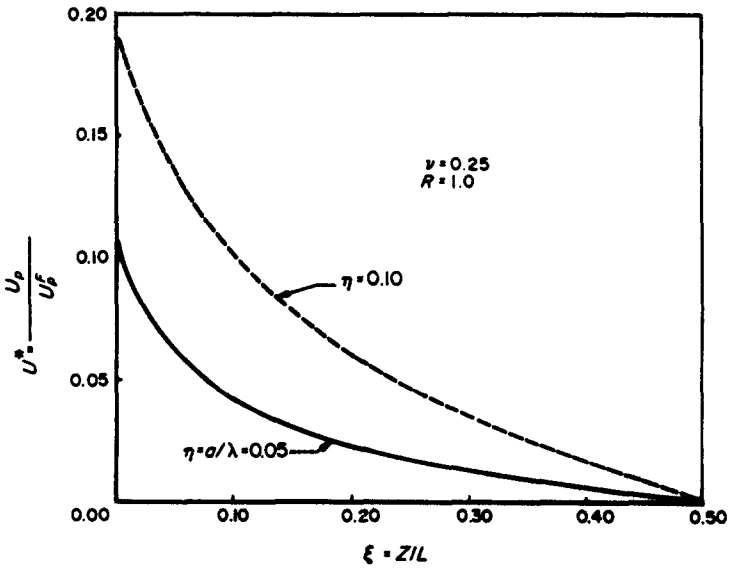

Fig. 6. Normalized displacement vs ξ, $R = 1.0$.

†All variations along the longitudinal axis are given in the range $0 \le \xi = z/L \le 0.5$. Values outside this range are merely Fourier extensions of the range.

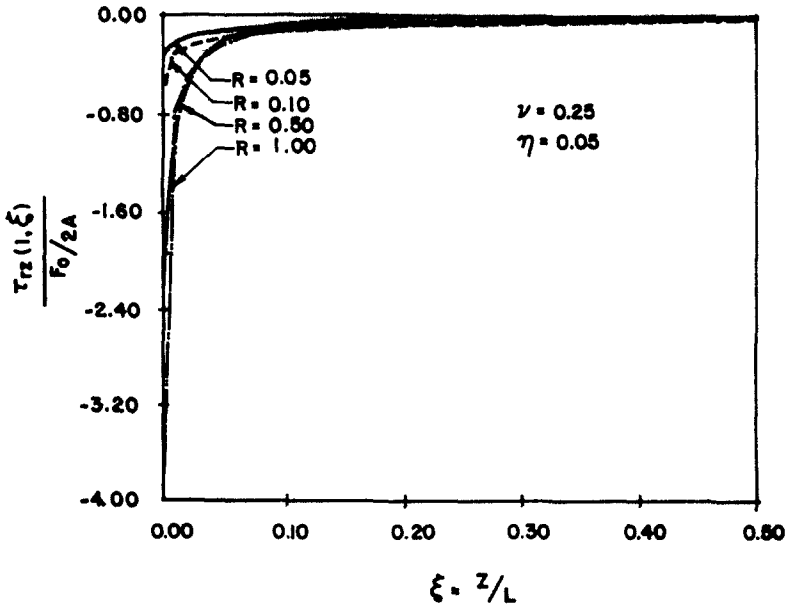

Fig. 7. Stress τ_{rz} vs ξ, $\eta = 0.05$.

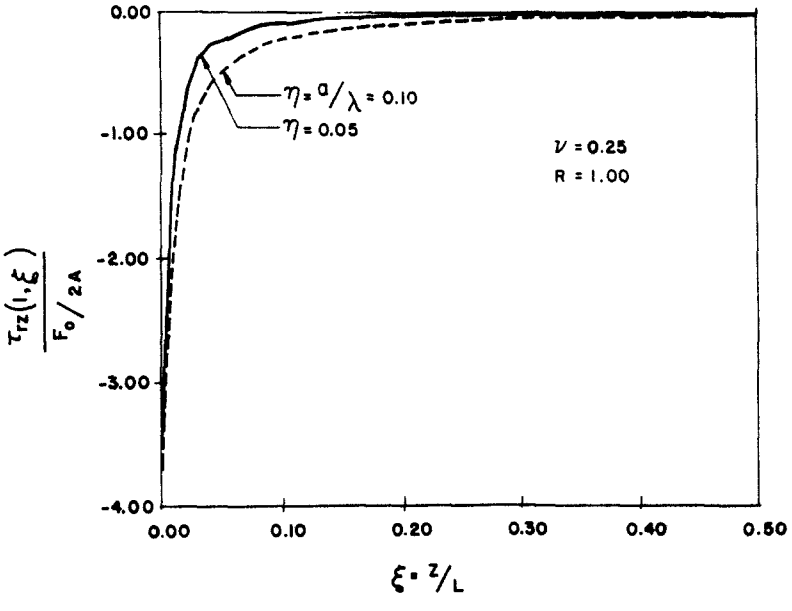

Fig. 8. Interacting shear stress vs ξ, $R = 1.01$.

application of the applied force F_0, and decays rapidly away from the applied load. Similar results are shown in Fig. 8 for typical values $\eta = 0.05$ and 0.1 for a fixed value $R = 1.0$. From these figures, it is evident that the interactive stress increases with both R and η. However this is not in contradiction with previous results, for although τ_{rz} increases with η, the longitudinal distance and hence the total area over which τ_{rz} acts decreases; hence as the relative interval between the applied forces F_0 increases, the total interaction is, in effect, weaker.

It should be noted that in both Figs. 7 and 8, the results at the value $\xi = 0$ are excluded since a singularity exists at this point. This may be demonstrated by considering the summation of eqn (22f) as m becomes large. Recalling that $v = 2\pi(2m - 1)\eta$ and noting, from the asymptotic

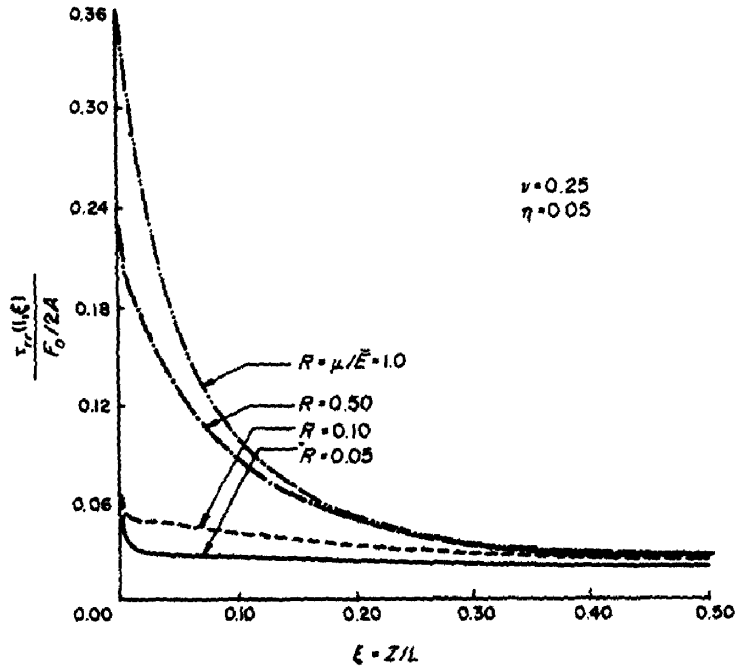

Fig. 9. Stress τ_{rr} vs ξ; $\eta = 0.05$

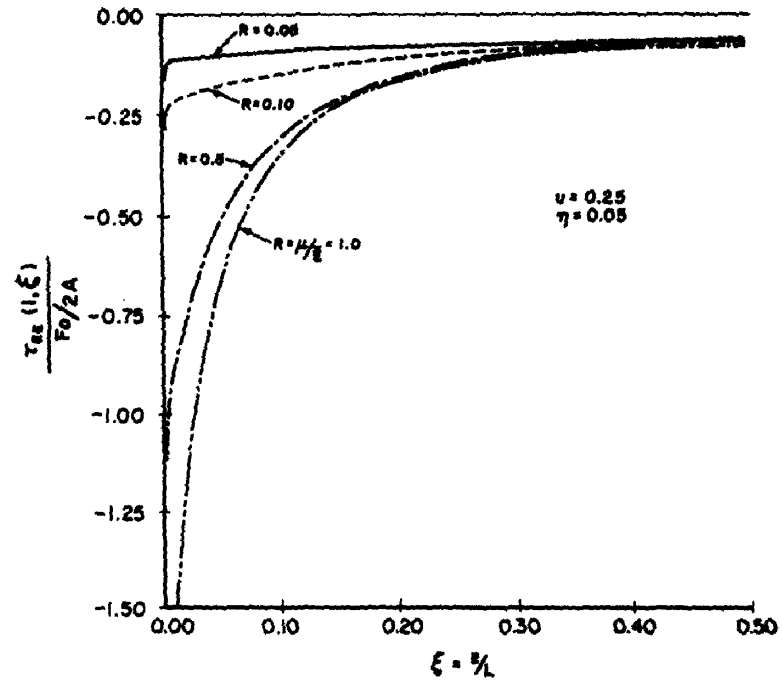

Fig. 10. Stress τ_{zz} vs ξ; $\eta = 0.05$.

expansions that

$$\lim_{v\to\infty} \frac{K_0(v)}{K_1(v)} = 1 - \frac{1}{2v} + \ldots \tag{28}$$

after some algebraic manipulation, one obtains

$$\lim_{v\to\infty} \frac{\tau_{rz}(1,\xi)}{F_0/2A} = \frac{-16(1-\nu)R}{(3-4\nu)\pi}\left[\cos\pi\xi + \frac{\cos 3\pi\xi}{3} + \frac{\cos 5\pi\xi}{5} + \ldots\right]. \tag{29}$$

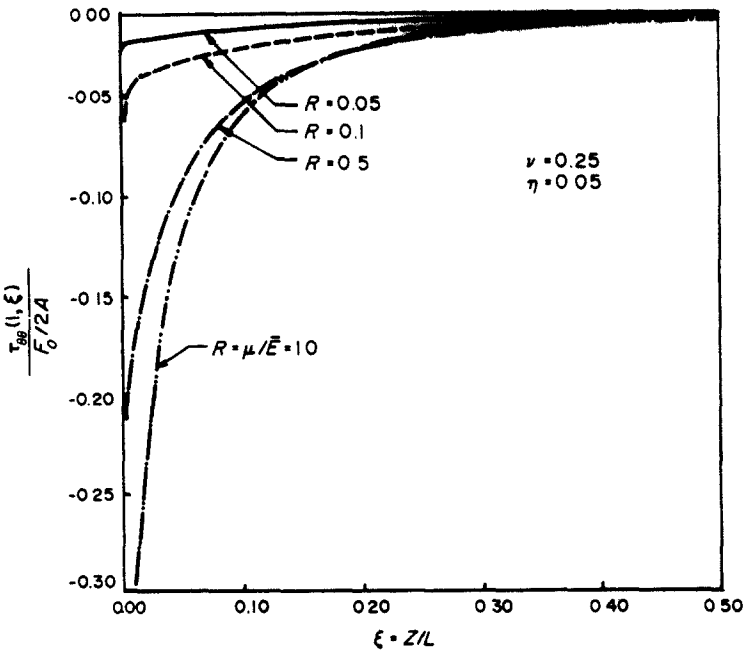

Fig. 11. Stress $\tau_{\theta\theta}$ vs ξ; $\eta = 0.05$.

Clearly, for $\xi = 0$, the series appearing in eqn (29) diverges, while for $0 < \xi < 1$, the series is seen to be convergent ([6], No. 505). Thus, eqn (22f) is not valid at $\xi = 0$. Similar singularities exist at $\xi = 0$ for the remaining stress components, and therefore the expression given by the remaining eqns (22) are valid only in the region $0 < \xi$.

Results for the remaining stress components τ_{rr}, τ_{zz} and $\tau_{\theta\theta}$ at $\rho = 1$ are presented in Figs. 9–11 respectively for typical values $\eta = 0.05$ and for stiffness ratios $R = 0.05, 0.1, 0.5$ and 1.0. In each case, the stress components are observed to decay rapidly at points away from the applied load.

It is noted that the results presented in Figs. 3–11 were given for a model in which concentrated forces F_0 are assumed to be acting, as shown in Figs. 1 and 2. Consequently to be consistent with de St.-Venant's principle, results have been given only for cases where $\eta = a/\lambda$ are small. However, if we now consider the case where the force F_0 is evenly distributed over the cross-section of the rod, solutions for large η become meaningful. Accordingly results for the displacement u^* are given in Figs. 12 and 13 for values $0 \leq \eta \leq 40$. The asymptotic

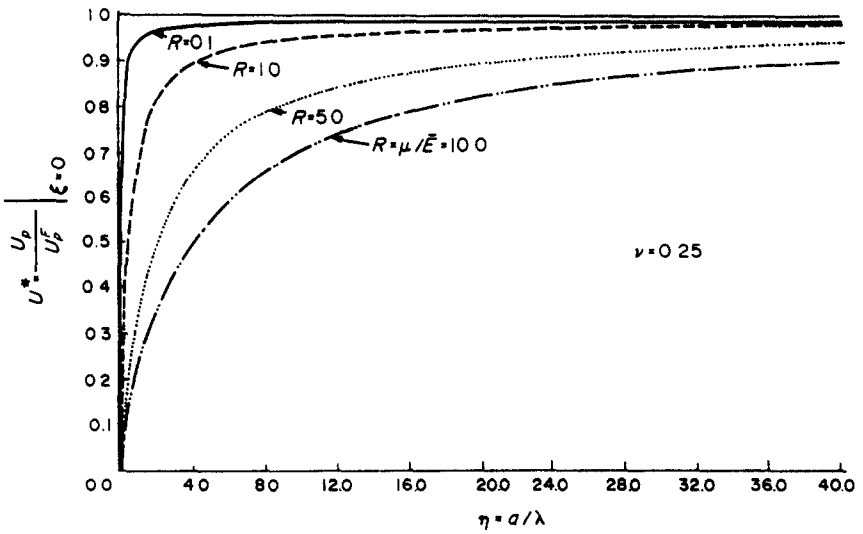

Fig. 12. Normalized displacements vs aspect ratio, extended range.

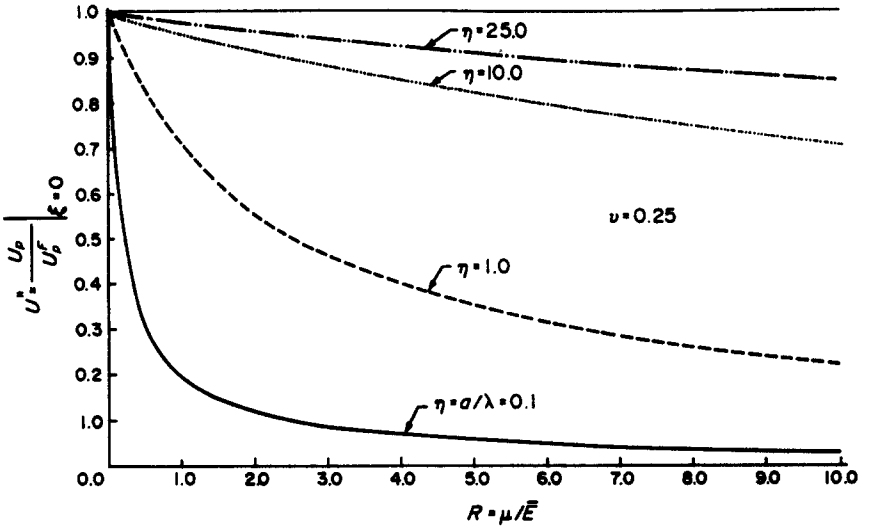

Fig. 13. Normalized displacement vs R.

behaviour of the rod, approaching that of a free rod unrestrained by the surrounding medium, is clearly seen as η becomes large.

REFERENCES

1. Proceedings of U.S.-Japan Seminar on Earthquake Engineering Research with Emphasis on Lifeline Systems, Tokyo (1976).
2. The current state of knowledge of lifeline earthquake engineering. *ASCE* (1977).
3. K. Toki and S. Takada, Earthquake response analysis of underground tubular structures. *Bull. Disas. Prev. Res. Inst.* 24(221), Kyoto University (June 1964).
4. Y. C. Fung, *Foundations of Solid Mechanics*, pp. 197–198. Prentice-Hall, Englewood Cliffs, New Jersey (1965).
5. C.-S. Yih, Solutions of the Hyper-Bessel equation, *Q. Appl. Math.* 13, 462–463 (1956).
6. L. B. W. Jolley, *Summation of Series*. Dover, New York (1961).